Modelling, Analysis and Mitigation of the Transformer Current Ringing in Dual Active Bridge Converters

Qin, Zian; Shen, Zhan; Blaabjerg, Frede; Bauer, Pavol

DOI
10.1109/ECCE.2018.8558016

Publication date
2018

Document Version
Final published version

Published in
2018 IEEE Energy Conversion Congress and Exposition, ECCE 2018

Modelling, Analysis and Mitigation of the Transformer Current Ringing in Dual Active Bridge Converters

Zian Qin[1], Zhan Shen[2], Frede Blaabjerg[2], Pavol Bauer[1]
Z.Qin-2@tudelft.nl
[1]Department of Electrical Sustainable Energy, Delft University of Technology, 2628 CD Delft, Netherlands
[2]Department of Energy Technology, Aalborg University, Aalborg 9220, Denmark

***Abstract*—Due to the parasitic capacitances of the transformer and inductor in Dual Active Bridge (DAB) converters, ringing may happen in the transformer currents especially when the transformer turns ratio is high. This high frequency current ringing may lead to EMI issues. It is found in this paper that the inductor connected on the low voltage side rather than the high voltage side of a DAB converter can help to mitigate the current ringing. The impedance of the magnetic tank is modelled to analyze the current ringing. The analysis is verified on a 2.5 kW DAB prototype.**

***Index Terms*— dual active bridge converter, parasitic capacitor, impedance model, current ringing, EMI**

I. Introduction

THE DAB converter, originally proposed in [1], is promising in applications like Electric Vehicle (EV) chargers, Solid State Transformers (SST) and DC grid systems [2-4], due to its simple topology and control, galvanic isolation, bidirectional power flow, wide input and output voltage adaptive range, high power density and efficiency. Nevertheless, the parasitic capacitance of its magnetic tank, as shown in Fig. 1, may lead to a low impedance at high frequency, which will then induce high frequency current ringing and worsen the EMI [5-7]. Meanwhile, wide-bandgap devices are being applied into the DAB converter for higher efficiency and higher power density [8], and high dv/dt caused by the fast switching of the wide-bandgap devices may make the current ringing and EMI issues even worse.

Analytical methods have been proposed to calculate the parasitic capacitance of the transformer [9]. Compared with it, the indirect measurement approach is easier [10]. The optimal design of planar transformers was given in [11], aiming to achieve the lowest ac resistance and leakage inductance. The cost was a higher parasitic capacitance compared with the non-interleaving PCB winding. Another winding design method was proposed in [12] to reduce the coupling capacitance between the primary and secondary windings by increasing their distance. But it made the manufacturing process much more complicated.

The parasitic capacitance of the inductor can affect the current ringing as well. The model of the inductor is relatively simpler, and the parasitic capacitance is mainly caused by the capacitance between the winding layers [9]. Therefore, the distance between the winding layers was increased to reduce the parasitic capacitance [6]. Another effective method was a single layer winding, and a vertical copper foil was applied to reduce the thickness of each turn and thereby make the single layer winding possible [7].

Nevertheless, no work can be found in literature so far to thoroughly analyze the transformer current ringing at a system level. Therefore, in this paper, the magnetic tank of the DAB converter is considered, instead of only the transformer or inductor. Since the current ringing is a kind of resonance, the impedance model of the magnetic tank is built for analysis. The paper is organized as following: the impedance analysis is shown in Section II, the experimental verifications are given in Section III and it is concluded in Section IV.

II. Impedance Analysis

As shown in Fig. 1, the magnetic tank of a DAB converter is composed of a transformer T and an inductor L_s connected in series. The transformer can be modelled as the circuit shown in Fig. 2, where C_H and C_L indicate the HV and LV side winding capacitors, respectively, C_{HL} depicts the coupling capacitor between the HV and LV side windings, $L_{m,L}$ represents the LV side magnetizing inductance of the transformer, $L_{leak,\mathrm{L}}$ demonstrates the equivalent leakage inductance of the transformer on LV side [10]. Since this paper is going to talk about the impact of the HV and LV side inductor on the current ringing, two equivalent circuits of the inductors are considered, as shown in Fig. 3 (a) for the HV side inductor and Fig. 3(b) for the LV side inductor. They have the same model, but different values of the elements, where $C_{ind,H}$ and $C_{ind,L}$ illustrate the winding parasitic capacitances of the HV and LV side inductors, respectively. In order to keep the impedance of the magnetic tank at the fundamental frequency unchanged, the inductances of the two inductors need to fulfill (1).

$$L_{ind,H} = n^2 L_{ind,L} \tag{1}$$

where n is the turns ratio of the transformer,

$$n = \frac{N_H}{N_L} \tag{2}$$

The LV side transformer current has a much higher ringing than the HV side, and the ringing happens only at the edge of the LV side pulsating voltage v_{CD} (the evidence will be shown in Section III). Therefore, only the LV side current ringing is analyzed, where the equivalent circuit of the current ringing can be shown as Fig. 4 (a), if an LV side inductor is applied. According to Thevenin's Theorem, the effect of the HV side

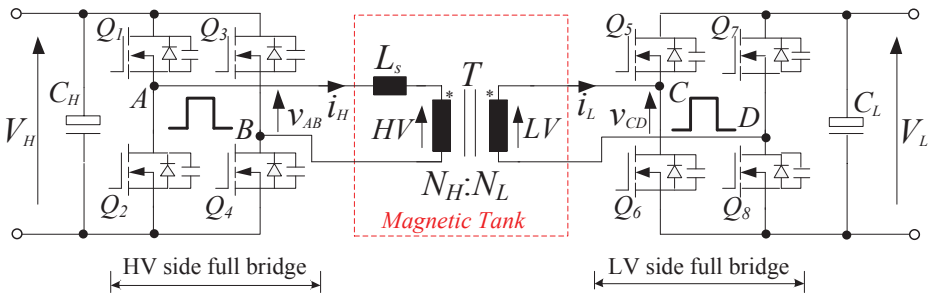

Fig. 1. A dual active bridge converter (DAB).

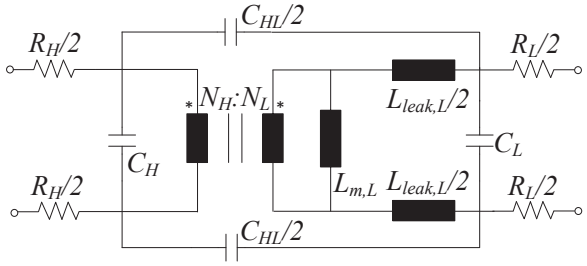

Fig. 2. Impedance model of a two-winding transformer.

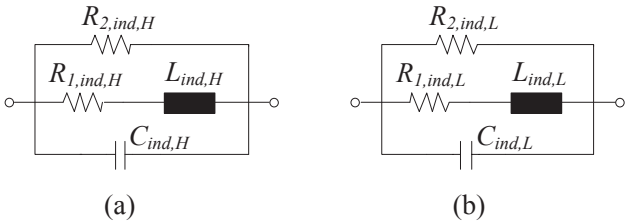

Fig. 3. Impedance model of (a) HV side (b) LV side inductor.

voltage can be eliminated by short-circuiting the HV side terminals. Moreover, all equivalent resistances are ignored since their impact is relatively small. Then C_H and $L_{m,L}$ are short-circuited, and the two winding coupling capacitances $C_{HL}/2$ are connected in parallel with the leakage inductances, as shown in Fig. 4 (b). Because $L_{leak,L}/2$ is much smaller than $L_{ind,L}$, it can be considered as short-circuit to further reduce the order of the model. Thus the model in Fig. 4 (c) is obtained and it is presented as,

$$Z_{in,LV,L_L} \approx L_{ind,L} // C_{ind,L} \tag{3}$$

Similarly, the equivalent circuit of the LV side current ringing is shown in Fig. 5 (a), if an HV side inductor is used. All the elements on the HV side are then equivalent to the LV side. The LV side equivalences of the $C_{ind,H}$ and C_H become $n^2 C_{ind,H}$ and $n^2 C_H$, respectively, and they are in parallel. The LV side equivalences of $L_{ind,H}$ is $L_{ind,H}/n^2$. Then the intermediate model in Fig. 5 (b) is obtained. Since $L_{leak,L}/2$ and $L_{m,L}$ are much smaller and larger than $L_{ind,H}/n^2$, respectively, they are considered as short- and open-circuit. Thus the intermediate model in Fig. 5 (c) is obtained. The LV side equivalence of the C_{HL} is relatively more difficult to obtain, and it is derived as the following,

$$C_{HL,LV} \frac{dv_{L,1}}{dt} = i_1 \tag{4}$$

where $C_{HL,LV}$ is the LV side equivalence of the C_{HL}, and i_1 is marked in the circuit in Fig. 5 (c). According to Kirchhoff's Current Law (KCL), it can be obtained as,

$$i_1 = i_{L,1} - i_{H,1} \tag{5}$$

where $i_{H,1}$ and $i_{L,1}$ are the HV and LV side winding currents, respectively, and their relationship can be expressed as,

$$i_{L,1} = i_{H,1} * n \tag{6}$$

For the coupling capacitor $C_{HL}/2$, it follows

$$\frac{C_{HL}}{2} \frac{d\frac{v_{H,1}-v_{L,1}}{2}}{dt} = i_{H,1} \tag{7}$$

where $v_{H,1}$ and $v_{L,1}$ are the HV and LV side winding voltages, respectively, and they follow

$$v_{H,1} = n * v_{L,1} \tag{8}$$

Substituting (4)-(6) and (8) into (7), it is obtained as,

$$C_{HL,LV} = \frac{(n-1)^2 C_{HL}}{4} \tag{9}$$

Thus, the simplified impedance model of the magnetic tank with HV side inductor from LV side is obtained as shown in Fig. 5 (d). Then according to (1), it is finally acquired,

$$Z_{in,LV,L_H} \approx L_{ind,L} // [n^2 (C_{ind,H} + C_H) + C_L + \frac{(n-1)^2 C_{HL}}{4}] \tag{10}$$

By comparing Z_{in,LV,L_H} in (10) with Z_{in,LV,L_L} in (3), it can be found that the input impedance of the magnetic tank from the LV side can always be simplified into a second-order model, where an equivalent inductor and capacitor are paralleled. The inductors are the equivalent ones of the HV or LV side inductor on LV side, so they are the same. But the equivalent capacitors are quite different. In Z_{in,LV,L_L}, it is only the winding capacitance of the LV side inductor $C_{ind,L}$. In Z_{in,LV,L_H}, it is a summation of the winding capacitance of the HV side inductor, the transformer, and the coupling capacitance of the transformer with different factors. Thus, it is much easier to achieve a lower equivalent capacitance in Z_{in,LV,L_L} by designing an inductor with small winding capacitance. But for Z_{in,LV,L_H} it needs to reduce the parasitic capacitance of not only the inductor but also the transformer. What's worse, the capacitances will be amplified by a factor n^2 or $(n-1)^2$ when

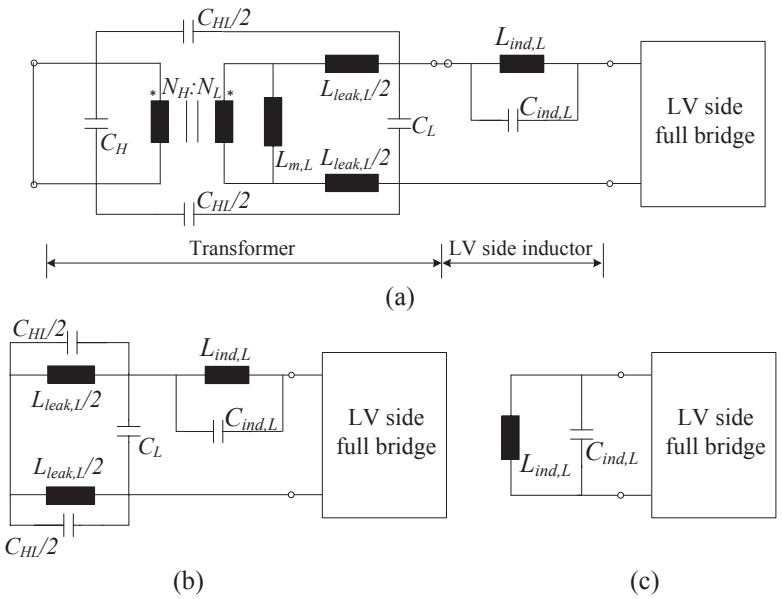

Fig. 4. LV side input impedance model of the magnetic tank with LV side inductor (a) detailed model (b) intermediate model (c) simplified model.

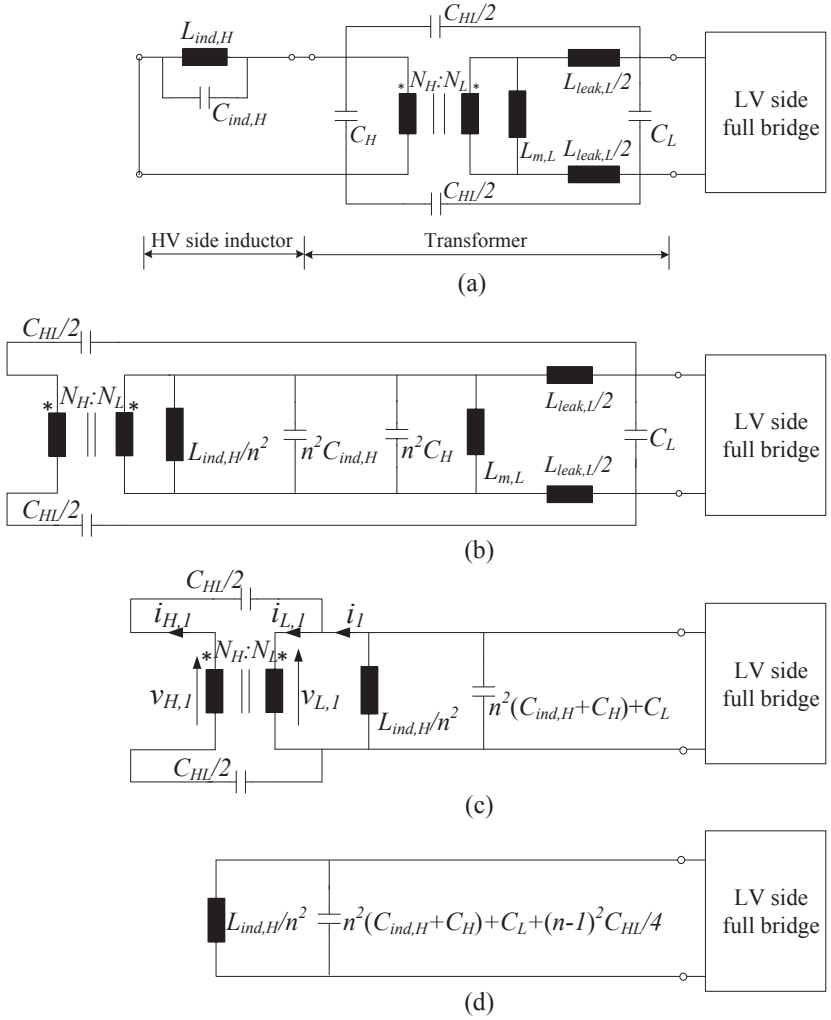

Fig. 5. LV side input impedance model of the magnetic tank with HV side inductor (a) detailed model (b) intermediate model 1 (c) intermediate model 2 (d) simplified model.

equivalent to the LV side. Consequently, Z_{in,LV,L_L} will have the same amplitude before the resonance frequency but higher amplitude after the resonance frequency than Z_{in,LV,L_H}, and in this way the high frequency current ringing is mitigated.

III. Experimental Verification

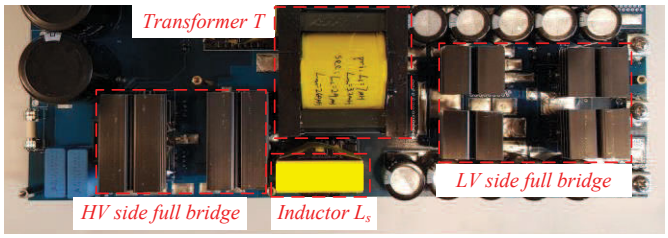

Fig. 6. A 2.5 kW dual active bridge converter prototype.

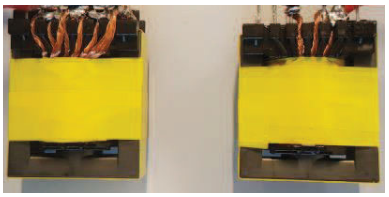

(a) (b)

Fig. 7. The picture of the (a) LV (b) HV side inductor.

In order to verify the analysis above, a 2.5 kW DAB prototype is built, as shown in Fig. 6. The switching frequency is 100 kHz, the nominal HV and LV side dc voltages are 400 V and 110 V, respectively. The turns ratio of the transformer is n = 3.5. The design parameters of the transformer are listed in Table I. By using a KEYSIGHT E4990A Impedance Analyzer and the measurement approach in [10], the parameters of the transformer impedance model are obtained and they are listed in Table III. The design parameters of the inductors L_h and L_l are listed in Table II. In order to make a fair comparison between the two inductors, the same type of cores are used, as shown in Fig. 7, and their windings are designed as a single layer to minimize the parasitic capacitance [7]. The impedances of the two inductors are measured and shown in Fig. 8. By fitting the curves based on the inductor impedance model in Fig. 3, the parameters of the model are obtained and they are listed in Table III. As seen, the inductor impedance model can match the measured impedance very well. Moreover, compared with the transformer, the winding capacitances of the inductors are much smaller even their turns are similar, which proves that the single layer winding approach is effective to reduce the parasitic capacitance. The input impedances of the magnetic network from LV side Z_{in,LV,L_H} and Z_{in,LV,L_L} are also measured and the amplitudes of the impedances are shown in Fig. 9. The fitting curves based on the simplified models of Z_{in,LV,L_H} and Z_{in,LV,L_L} in (10) and (3) are also shown. As seen, the simplified models can match the measured impedances well before the second resonance frequency, which is 6 MHz in Z_{in,LV,L_H} and higher than 30 MHz in Z_{in,LV,L_L}. The amplitude of the fitting curve is higher

TABLE I. DESIGN PARAMETERS OF THE TRANSFORMER.

	Transformer T
Core type	ETD 59
Core material	Ferrite N97
Primary winding	Litz wire Ø 0.2 mm, 90 strands in parallel, 21 turns
Secondary winding	Copper foil 0.15 mm x 35 mm, 2 layers in parallel, 6 turns

TABLE II. DESIGN PARAMETERS OF THE INDUCTORS.

	Inductor L_H	**Inductor L_L**
Core type	ER42V (gapped)	
Core material	Ferrite N87	
Winding	Litz wire Ø 0.2 mm	
	90 strands in parallel, 17 turns	270 strands in parallel, 5 turns

TABLE III. MEASURED PARAMETERS OF THE TRANSFORMER AND INDUCTORS

	C_H	C_L	C_{HL}	$L_{leak,L}$	$L_{m,L}$
Transformer	77 pF	253 pF	106 pF	0.24 uH	202 uH
	$R_{2,ind,H}$	$R_{1,ind,H}$	$L_{ind,H}$	$C_{ind,H}$	
Inductor L_H	6.5 k Ω	11.5 m Ω	37.5 uH	5.5 pF	
	$R_{2,ind,L}$	$R_{1,ind,L}$	$L_{ind,L}$	$C_{ind,L}$	
Inductor L_L	0.6 k Ω	8.5 m Ω	3.5 uH	22 pF	

than the measured curve at the first resonance frequency because all the damping resistances are ignored in the simplified impedance model. But it will not affect the current ringing analysis, since the impedance has a peak value at the first resonance frequency and the current ringing would not happen at this frequency. Due to the larger parasitic capacitance, Z_{in,LV,L_H} has a lower amplitude than Z_{in,LV,L_L} in the range between its first and second resonance frequency, which increases the chance of current ringing. Actually, the test results in Fig. 10 (c) show that the current ringing happens at 4 MHz, which is between the first and second resonance frequency of Z_{in,LV,L_H}. In detail, at 4 MHz the impedance amplitudes of Z_{in,LV,L_H} and Z_{in,LV,L_L} are 20 Ω and 100 Ω, respectively. Thus the current ringing is much mitigated when the HV side inductor is replaced by the LV side inductor, as shown in Fig. 10 (b). Moreover, the HV side current ringing is always small no matter the HV or LV side inductor is used. The measured efficiency in Fig. 11 shows that with a proper design the HV and LV side inductor can have very similar power loss.

IV. Conclusions

In this paper, the current ringing issue in the DAB converter is analyzed by means of the impedance model of the magnetic tank. It is found that if the DAB converter has a transformer

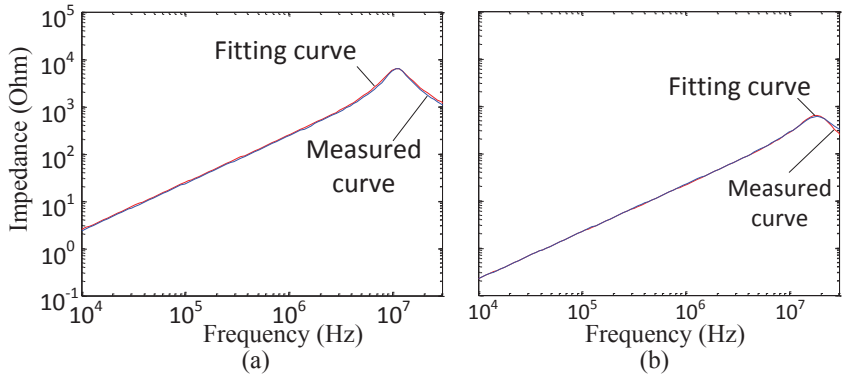

Fig. 8. Impedance amplitude of the (a) HV (b) LV side inductor.

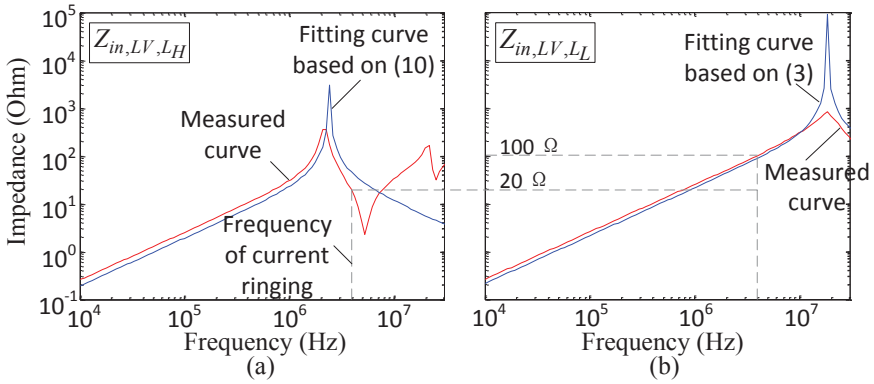

Fig. 9. Input impedance amplitude of the magnetic network with (a) HV (b) LV side inductor, from LV side.

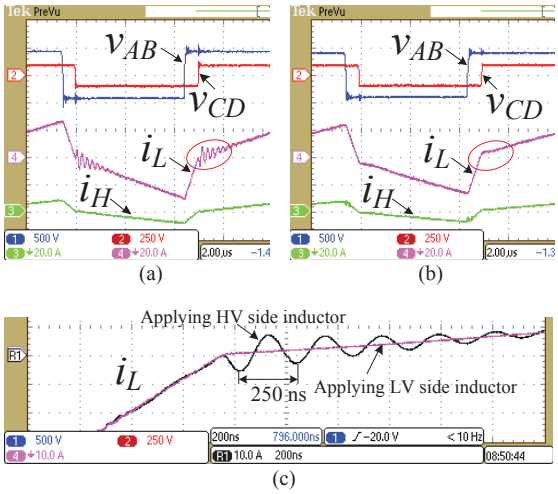

Fig. 10. Experimental results to show LV side transformer current with (a) HV side inductor (b) LV side inductor.

with a high turns ratio, then a low voltage side rather than a high voltage side inductor can help to mitigate the current ringing effectively. Moreover, the impact of the parasitic capacitances of the transformer can be much reduced. As a result, the EMI issue caused by the high frequency current ringing can be alleviated and the design challenge of the magnetic tank can be lowered.

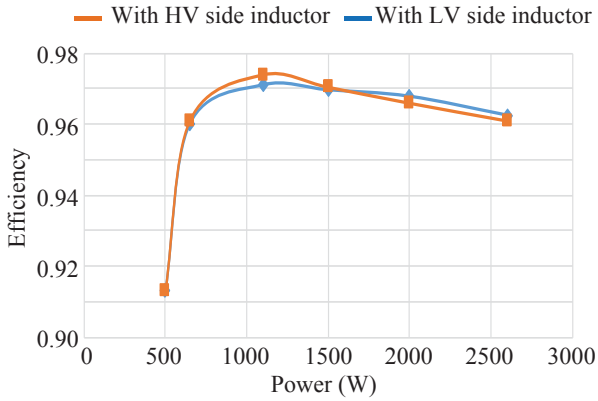

Fig. 11. The efficiency of the converter with HV and LV side inductor.

REFERENCES

[1] R. W. De Doncker, D. M. Divan, and et. al, "A Three-Phase Soft-Switched High Power Density DC/DC Converter for High Power Applications," in Proc. of IEEE Industry Applications Society Annual Meeting, vol. 1, Oct. 1988, pp. 796–805.

[2] G. Ortiz, C. Gammeter, J. W. Kolar, and et. al, "Mixed MOSFET-IGBT bridge for high-efficient medium-frequency dual active-bridge converter in solid state transformers," in Proc. of COMPEL 2013, pp. 1–8, 2013.

[3] S. Anwar, W. Zhang, F. Wang, and et. al, "Integrated dc-dc converter design for electric vehicle powertrains," in Proc. of APEC 2016, pp. 424–431, 2016.

[4] S. P. Engel, M. Stieneker, N. Soltau, and et. al, "Comparison of the modular multilevel dc converter and the dual-active bridge

converter for power conversion in HVDC and MVDC grids," IEEE Trans. Power Electron., vol. 30, no. 1, pp. 124–137, 2015.
[5] R. T. Naayagi, "Electromagnetic compatibility issues of dual active bridge DC-DC converter," in Proc. of ICEETS' 2013, pp. 699-703, 2013.
[6] M. Zdanowski, J. Rabkowski, K. Kostov, and et. al, "Design and Evaluation of Reduced Self-Capacitance Inductor in DC/DC Converters with Fast-Switching SiC Transistors," IEEE Trans. Power Electron., vol. 29, no. 5, 2014.
[7] J. C. Hernandez, L. P. Petersen, M. A. E. Andersen, "Low Capacitive Inductors for Fast Switching Devices in Active Power Factor Correction Applications," in Proc. of IPEC' 2014, pp. 3352-3357, 2014.
[8] L. Xue, Z. Shen, D. Boroyevich, and et. al, "Dual Active Bridge-Based Battery Charger for Plug-in Hybrid Electric Vehicle With Charging Current Containing Low Frequency Ripple," IEEE Trans. Power Electron., vol. 30, no. 12, pp. 7299-7307, 2015.
[9] J. Biela, and J. W. Kolar, "Using transformer parasitics for resonant converters—A review of the calculation of the stray capacitance of transformers," IEEE Trans. Ind. Appl., vol. 44, no. 1, pp. 223–233, Jan./Feb. 2008.
[10] H.-Y. Lu, J.-G. Zhu, and S. Y. R. Hui, "Experimental determination of stray capacitances in high frequency transformers," IEEE Trans. Power Electron., vol. 18, no. 5, pp. 1105–1112, Sep. 2003.
[11] Z. Ouyang, O. C. Thomsen, and M. A. E. Andersen, "Optimal design and tradeoff analysis of planar transformer in high power dc–dc converters," IEEE Trans. Ind. Electron., vol.59, no.7, pp. 2800-2810, July 2012.
[12] K. Nguyen-Duy, Z. Ouyang, A. Knott, and et. al, "Minimization of the transformer inter-winding parasitic capacitance for modular stacking power supply applications," in Proc. of EPE' 2014, pp. 1-10, 2014.